**APATITE MICROSTRUCTURES AND ITS VOLATILE COMPOSITION IN EUCRITES.** T. J. Barrett[1], A. Černok[1,2], G. Degli-Alessandrini[1], M. Anand[1,3], I. A. Franchi[1] and J. Darling[4]. [1]School of Physical Sciences, The Open University, Walton Hall, Milton Keynes, MK7 6AA, UK (E-mail: thomas.barrett@open.ac.uk), [2]Centre for Applied Planetary Mineralogy, Department of Natural History, Royal Ontario Museum, Toronto, M5S 2C6, Canada [3]Department of Earth Sciences, Natural History Museum, London, SW7 5BD, UK, [4]School of Earth & Environmental Sciences, University of Portsmouth, Portsmouth, PO1 3QL, UK.

**Introduction:** Apatite is a common phosphate mineral in planetary materials known to contain appreciable amounts of volatiles (F, Cl, OH) [e.g. 1-4]. As such, apatite has recently been of significant interest in assessing the volatile evolution of various bodies within the Solar System via *in-situ* analysis (e.g. [5-7]). Whilst these works account for the textural context of the apatite grain and the surrounding mineralogy, less attention has been given to understanding as to how the structure of grains may be influenced by metamorphism and shock deformation.

Electron Backscatter Diffraction (EBSD) analyses provide structural information at the µm and sub-µm length scales. In extraterrestrial samples, it has mostly been used to interpret larger-scale plastic deformation [8] and shock deformation in geochronometers such as zircon and baddeleyite [e.g. 9-11]. Importantly, these studies highlight the importance of understanding deformation at the µm-scale when interpreting complex U-Pb data and the mobility of Pb, a moderately volatile element. As yet, there have been no studies of how deformation-induced microstructures may influence the isotopic composition of volatiles in apatite in eucrites.

In this study we investigate the microstructure of apatite grains in eucrites for which H and Cl isotopic composition have been previously reported [12, 13], in order to explore the relationship between crystallographic features of apatite and its volatile content and isotopic composition in eucrites of different shock grades.

**Samples:** The samples analysed here with prior isotopic data are the basaltic eucrites: Dar Al Gani (DaG) 844, Millbillillie, Stannern and Sioux County and the residual eucrite DaG 945. These samples have been assigned shock grades of S1 and S2 [14, 15] based on optical microscopy of studied sections and the literature data [16]. Metamorphic grades range from type 4 to type 6 [17, 18]. Additional samples (Puerto Lápice and Padvarninkai), for which no volatile data currently exist, were selected to explore samples that have experienced higher shock stages (S3-S5)[19, 20].

**Methods:** The lattice orientation and internal microstructure of apatite grains were investigated using EBSD on a Zeiss Supra 55VP FEG-SEM equipped with an Oxford Instruments EBSD detector located at The Open University (OU). The step size used ranged from 300 nm to 750 nm with binning ranging from 2 × 2 pixels to 4 × 4 pixels. Generated Electron Backscatter Patterns (EBSPs) were matched to a hexagonal unit cell [21]. Results were processed using Oxford Instruments HKL Channel 5 software.

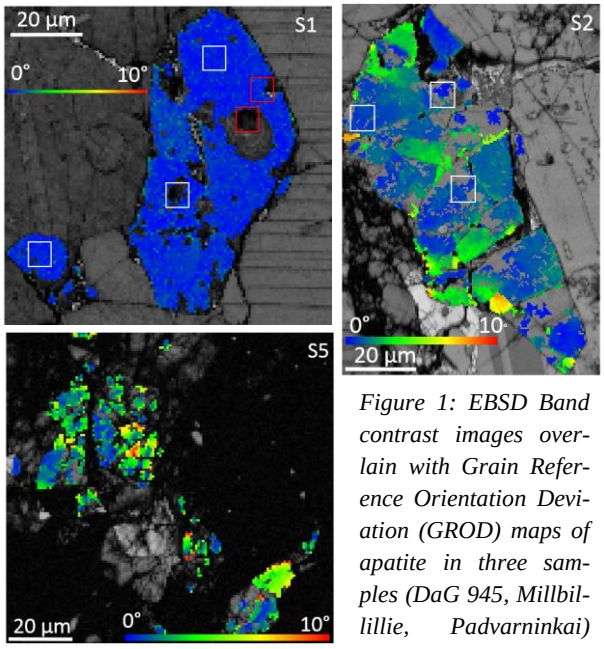


*Figure 1: EBSD Band contrast images overlain with Grain Reference Orientation Deviation (GROD) maps of apatite in three samples (DaG 945, Millbillillie, Padvarninkai) that have experienced three different shock stages (S1, S2 and S5, resp.). White squares indicate H isotope NanoSIMS pits [13] whereas red squares indicate Cl isotope pits [14].*

**Results and Discussion:** EBSD maps were collected for 23 apatite grains from six eucrites. Microstructures in apatite become progressively more complex with increasing shock deformation (Fig.1). Apatite in DaG 945, showing S1 shock-stage, occur as single crystals with no obvious signs of internal deformation in EBSD images. GROD maps locate subgrains within the indexed grain, and then the orientation of each pixel relative to the subgrain average is color-coded (Fig. 1). For S1, GROD maps show no subgrain formation and low to no misorientation. S2 samples begin to show brecciation and incipient fracturing of minerals. These mechanically broken blocks typically show very low degrees of intragranular crystal-plastic deformation (typically up to 3°). DaG 844 (S2), however, does not

produce EBSD patterns at the length scales of our analyses. Raman spectra of the apatite grains indicate that grains are well-crystallised and not amorphous. As apatite grains in this sample are small compared to apatite in other samples of the same shock grade (~ 10 µm in the longest direction) it is possible that the fracturing of the grains into small pieces during shock deformation results in poor band contrast images. At the highest levels of shock deformation (S5) apatite is in contact with a diaplectic plagioclase glass and reveals a fine, granular interior, subgrain formation, and a general increase in misorientation (up to ~ 6.5°) (Fig.1).

The H isotopic composition of apatite grains analysed for samples displaying S1 and S2 shock-deformation stages, appears invariant (Fig. 2). Stannern and Millbillillie (both S2) contain apatite with both high and low $H_2O$ content and would, therefore, suggest that $H_2O$ content is also not linked to shock-stage. Brecciation, mineral fracturing, and local misorientation does not seem to affect the abundance or isotopic composition of the samples. As each apatite grain appears to be a single crystal, with fragments predominately arising from mechanical fracturing, shock cannot be used to explain any intra-grain variation of $H_2O$ seen within apatite either. It is likely, therefore, this variation is primary in nature.

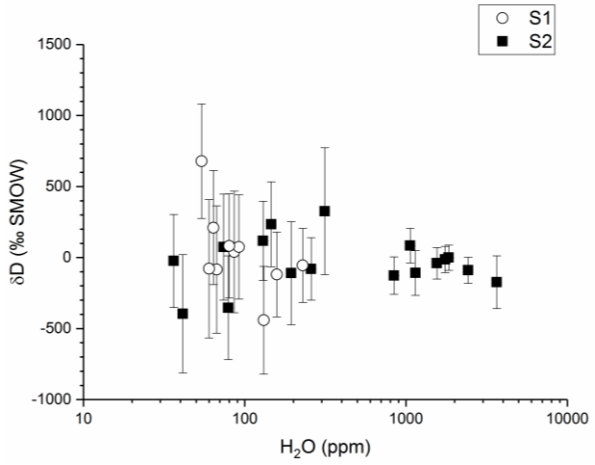


*Figure 2: Comparison between $H_2O$ content and δD value for apatite from eucrite samples displaying different shock grades. Uncertainties are 2σ. Volatile data from [13].*

Chlorine isotopes in apatite also do not seem to be altered by shock deformation with the majority of basaltic eucrites (shock stages S1 and S2) having $\delta^{37}Cl$ values ranging between ~ - 1‰ and + 3 ‰.

Care should be taken when interpreting volatile data in these samples owing to the fact that the majority of eucrites have undergone at least some thermal metamorphism which could also have affected their isotopic composition. DaG 945 in particular, whilst retaining some primary magmatic zoning in pyroxene and plagioclase [22], has experienced short periods of high-temperature heating and localized recrystallisation. This sample is consistent with other eucrites for its apatite H isotopic composition but has an anomalously heavy Cl isotope composition [14]. Analysed apatite do not appear to be located in recrystallised areas and there are no obvious unusual microstructures (in band contrast, GROD etc.) for these apatite grains that would indicate that this value is not primary in origin (S1 map in Fig. 1).

**Conclusions:** There is currently no obvious link between isotopic composition and apatite shock states S1 and S2 or thermal metamorphic grade. Targeted isotopic analysis of apatite with EBSD maps in samples with higher shock grades (S3-S5) is in progress to expand the dataset and include samples displaying a wider range of shock stages.

**References:** [1] Sarafian A. R. et al. (2017) *EPSL* 459:331-319. [2] Barnes J. J. et al (2014) *EPSL* 390:244-252. [3] Bellucci J. J. et al (2017) *EPSL* 458:192-202. [4] Hallis L. J. et al. (2012) *EPSL* 359-360:84-92. [5] Hallis L. J. et al. (2017) *Philos. Trans. R. Soc. A* 375. [6] Shearer C. K. (2018) *GCA* 234:24-36. [7] Robinson K. L. et al. (2016) *GCA* 188:244-260. [8] Tkalcec B. J. & Brenker F. E. (2014) *MAPS* 49(7):1202-1213. [9] Darling J. R. et al. (2016) *EPSL* 444:1-12. [10] White L. F. et al (2017) *Nat. Commun.* 8:15597. [11] White L. F. et al (2018) *Geology* 46:719-722. [12] Barrett T. J. et al. (2016) *MAPS* 51:1110-1124. [13] Barrett T. J. et al. *In review.* [14] Stöffler D. et al. (1991) *GCA* 55:3845-3867. [15] Fritz J. et al. (2017) *MAPS* 52(6):1216-1232. [16] Meteoritical Bulletin Database [17] Takeda H. & Graham A. L. (1991) *Meteoritics* 26(2):129-134. [18] Yamaguchi A. et al. (1996) *Icarus* 124:97-112. [19] Llorca J. et al. (2009) *MAPS* 44:159-174 [20] Bischoff A. & Stöffler D. (1992) *Eur. J. Mineral.*, 4,707-755. [21] Wilson R. M. et al. (1999) *Am. Min.* 84:1406-1414. [22] Yamaguchi A. et al. (2009) *GCA* 73:7162-7182.

**Acknowledgements:** We thank the following individuals and institutions for providing polished thin-sections: Smithsonian Institution: Padvarninkai (USNM 5946) and Sioux County (USNM 896 2), Western Australia Museum: Millbillillie (13357.3), Naturhistorisches Museum Wien: Stannern (L4979), Institut für Planetologie Münster: Puerto Lápice. A.C. received funding from the European Union's Horizon 2020 research and innovation program under grant agreement No 704696.